Geophysical Research Letters

RESEARCH LETTER
10.1029/2024GL114186

Characterization of Convection and Rainfall Off the Pacific Coast of Colombia Using Airborne Radar and Dropsonde Data

D. J. Raymond[1] and **Ž. Stone**[1]

[1]Physics Department and Climate and Weather Consortium, New Mexico Tech, Socorro, NM, USA

Key Points:

- Dropsondes and airborne Doppler radar were used to document convection off the Colombian Pacific coast from high altitude
- Radar distinguished aggregates from graupel in clouds by a step increase in particle fall speed at the freezing level
- Dropsonde analysis showed that aggregates occurred in a variety of active convective systems, not just decaying stratiform

Correspondence to:
D. J. Raymond,
david.raymond@nmt.edu

Citation:
Raymond, D. J., & Stone, Ž. (2025). Characterization of convection and rainfall off the Pacific coast of Colombia using airborne radar and dropsonde data. *Geophysical Research Letters*, *52*, e2024GL114186. https://doi.org/10.1029/2024GL114186

Received 9 DEC 2024
Accepted 28 MAR 2025

Author Contributions:
Conceptualization: D. J. Raymond, Ž. Stone
Data curation: D. J. Raymond
Funding acquisition: Ž. Stone
Methodology: D. J. Raymond
Project administration: Ž. Stone
Resources: Ž. Stone
Software: D. J. Raymond
Writing – original draft: D. J. Raymond
Writing – review & editing: Ž. Stone

Abstract The Organization of Tropical East Pacific Convection project used dropsondes deployed from high altitude and a downward-pointing W-band Doppler radar to document the characteristics of mesoscale convective systems (MCSs) located over the Pacific coastal waters of Colombia. MCSs dominated by ice crystal aggregates above the freezing level rather than graupel, as shown by the radar, are generally thought to indicate decaying stratiform rain systems with only light rain. However, dropsonde grids showed a broader range of MCS types in this category, some with shallow convection producing intense rainfall. The radar had difficulty in distinguishing between different types of aggregate-dominated MCSs.

Plain Language Summary We used the National Science Foundation/National Center for Atmospheric Research Gulfstream-V aircraft to overfly atmospheric convection over the Pacific coastal waters of Colombia. Dropsondes that radio back temperature, humidity, and winds to the aircraft were deployed in a grid pattern to map out the state of the atmosphere in and around convection. In addition, a downward-pointing radar observed patterns and types of precipitation produced by the convection. We found that some convection produced mainly aggregates of ice crystals (snowflakes) above the freezing level whereas others were dominated by graupel particles (tiny hailstones). The former are generally thought to produce only light rain, but we found otherwise—some convection dominated by aggregates produced heavy rainfall at the surface. The radar had difficulty in distinguishing between the low and high rainfall cases. This is an important finding, because satellite borne radars would likely have the same problem. Such radars are an important part of the system producing input data for use in global weather and climate models.

1. Introduction

Houze et al. (2015) documented the character of mesoscale convective systems (MCSs) over a broad region of the tropics using the precipitation radar on the Tropical Rainfall Measuring Mission (TRMM) satellite. This Ku-band radar used reflectivity patterns to categorize MCS convection into deep convective cores and wide convective cores. Deep convective cores were typically observed over land, whereas wide convective cores were more commonly seen over the ocean. In addition, broad stratiform regions were identified, either as elements of convective systems or as stand-alone entities.

Some of the most interesting cases of this study occurred off the Pacific coast of Colombia, a region of very high annual rainfall (Houze et al., 2015; Jaramillo et al., 2017; Poveda, 2023; Poveda & Mesa, 2000; Sakamoto et al., 2011). In particular, Houze et al. (2015) noted that a possible ambiguity existed with broad stratiform regions between classical stratiform rain conditions with little or no active convection and regions which contained widespread shallow convection in addition to stratiform rain. The distinction is important because the former exhibit mainly weak precipitation over a broad area whereas the latter have the potential of producing significant additional precipitation from shallow convection. The two also can differ greatly in their vertical mass fluxes, and hence in their convective heating profiles, which has strong implications for their effect on global flow patterns.

Observations of convection over the tropical east Pacific and southwest Caribbean, including off the Pacific coast of Colombia, were made during August and September of 2019 during the Organization of Tropical East Pacific Convection (OTREC) project. Dropsondes deployed at high altitude from the US National Science Foundation/National Center for Atmospheric Research Gulfstream-V (NSF/NCAR G-V) aircraft in a nearly uniform grid allowed mass flux profiles as well as the vertically integrated moisture convergence to be measured on a 1° scale

Table 1
Case Studies of Mesoscale Convective Systems Observed Off the Pacific Coast of Colombia

Case	(Longitude, latitude)	SST (C)	S_m (mm/d)	Mass flux	Radar; sat (UTC)
0811	(−78.0, 5.0)	26.8	28	Bimodal	
0816*	(−78.5, 6.3)	26.9	124	Bottom-heavy	1452–1508; 1500
0825*	(−79.0, 7.0)	27.1	−42	Stratiform	1526–1543; 1600
0909*	(−78.5, 5.5)	27.2	38	Bimodal	1830–1910; 1900
0917*	(−78.5, 5.8)	26.8	148	Deep	1640–1653; 1700
0922	(−79.5, 6.5)	27.3	47	Deep	
0925	(−80.2, 7.0)	27.7	221	Bottom-heavy	

Note. Asterisks indicate cases presented in this paper. The date is incorporated in the case name in the form of (mmdd). S_m is the vertically integrated moisture convergence in precipitation units. The fifth column gives a brief description of the form of the mass flux profile while the last column shows the radar averaging interval and the satellite image times in Figure 1.

(Fuchs-Stone et al., 2020; Raymond & Fuchs-Stone, 2021; Raymond et al., 2024). In addition to the dropsondes, the downward-pointing W-band Hiaper Cloud Radar allowed the fall velocity and reflectivity of precipitation to be determined, at least above the freezing level where attenuation is small.

Raymond et al. (2024) looked in detail at MCSs during OTREC. Here we choose 4 representative cases located in the Pacific coastal region of Colombia and analyze them using satellite, airborne radar, and dropsonde data sets.

Section 2 provides a brief summary of the data and its analysis. Results are described in Section 3. Section 4 discusses these results and presents the conclusions.

2. Data and Analysis

Dropsondes were deployed on an approximate 1° × 1° Cartesian grid off the Pacific coast of Colombia from approximately 13 km above sea level. The grid pattern covered a rectangular longitude-latitude domain of [−81°, −78°] by [4°, 7°], with the eastern edge being very close to the Colombian coast. A three-dimensional variational scheme (3DVar) was used on the dropsonde winds and thermodynamic data. This scheme minimizes a cost function that enforces mass continuity, a match to the soundings, and incorporates smoothing on the scale of the sonde separation. No background field from large scale analysis is included in order to avoid introducing model biases. See Fuchs-Stone et al. (2020) and Raymond and Fuchs-Stone (2021) for more detail.

Downward-pointing, earth-relative Doppler velocity rays corrected for unfolding, pointing errors, and aircraft motion were provided by the Earth Observing Laboratory of NCAR. These fields were decimated to 1 s intervals in time (≈200 m in horizontal spacing) and 200 m in range for presentation purposes, producing frequency distributions of height versus fall velocity and reflectivity. Normalization of the plots was adjusted to bring out weaker features, resulting in saturation for stronger features. Particle fall velocity profiles provided an excellent tool for distinguishing between graupel and unrimed ice crystal aggregates, as slowly falling aggregates rapidly melt and contract into more rapidly falling liquid drops at the freezing level. Graupel particles have much higher density and do not melt rapidly when passing through the freezing level and therefore do not show a step function increase in fall velocity at this level.

Infrared satellite images from GOES-16 were used to examine the evolution of MCSs in the OTREC area. Data from the GOES Geostationary Lightning Mapper were used to determine whether the systems in question produced lightning.

3. Results

Table 1 shows the dates and locations of the 7 MCSs documented in the Pacific coastal region of Colombia by Raymond et al. (2024) in their Table 1. Of the 7 cases, 2 have bottom-heavy mass flux profiles, 2 have deep mass flux profiles with strong mass fluxes from low levels to the upper troposphere, one is characteristic of stratiform rain with upward mass flux in the upper troposphere and downward mass flux in the lower troposphere, and 2

10.1029/2024GL114186

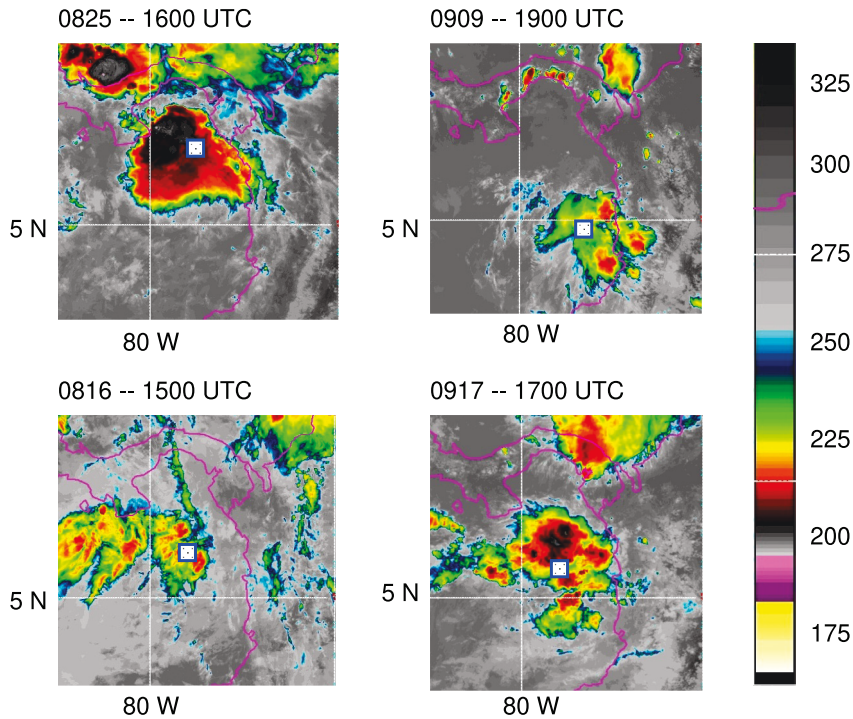

Figure 1. Infrared satellite images of the 4 mesoscale convective systems selected for study at the approximate times at which they were observed by the G-V (see Table 1). The white-filled blue squares show the locations of the averaged radar profiles and the 3DVar soundings and mass flux profiles. The Kelvin brightness temperature scale is on the right.

have a bimodal structure with a combination of stratiform conditions in the upper troposphere and redeveloping shallow convection below.

Table 1 also shows the sea surface temperatures (SSTs) and the vertically integrated moisture convergence for each case. The moisture convergence plus the surface moisture flux equals the precipitation rate in the steady state. Since we do not have quantitative information on the time dependence of the systems, we present only the moisture convergence.

The asterisks in Table 1 indicate those cases selected for study in this paper. Case 0816 is chosen to represent bottom-heavy mass flux cases, 0909 represents bimodal cases, and 0825 and 0917, respectively represent stratiform and deep mass fluxes. Figure 1 shows infrared satellite snapshots of the 4 cases taken at the approximate times at which they were observed by the G-V. Soundings and mass flux profiles were taken from the 3DVar analyses at the locations of the white squares. However, keep in mind that these really represent average values on the scale of about 1°, so the precise sampling location within this range is not important.

Figures 2–5 present information on the 4 cases. In each case the first panel from the left shows the frequency distribution of precipitation in fall velocity-height space obtained from a G-V pass through the system, with stronger yellow values representing more precipitation. The horizontal red line represents the approximate height of the freezing level. The second panel shows the radar reflectivity distribution as a function of height. The third panel presents the sounding from the 3DVar analysis in terms of the moist entropy (blue) and the saturated moist entropy (red). The vertical black line represents the entropy of a parcel ascending from the boundary layer. The difference between the parcel's entropy value and the saturated moist entropy of the environment is an approximate measure of the parcel buoyancy above the parcel's condensation level. The fourth panel shows the mesoscale vertical mass flux from the 3DVar analysis.

3.1. 0825

The case presented in Figure 2 is that of a classic stratiform rain region (Houze, 1977; Houze & Betts, 1981; Leary & Houze, 1980; Zipser, 1969, 1970, 1977). Consistent with the cited literature, the fall velocity pattern is

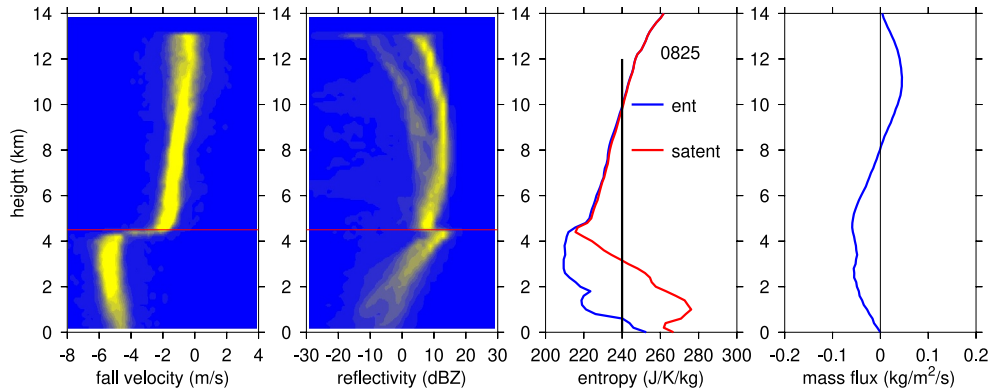

Figure 2. Case 0825. First panel from left: Frequency distribution of hydrometeors as a function of fall velocity and height. Second panel: Frequency distribution as a function of reflectivity and height. Third panel: 3DVar sounding sampled at the white square in Figure 1 in terms of moist entropy (blue) and saturated moist entropy (red). The black line shows the entropy of an ascending boundary layer parcel. The difference between this and the saturated moist entropy (red line) is a measure of parcel buoyancy. Fourth panel: 3DVar mass flux profile.

characteristic of unrimed ice crystals and aggregates above the freezing level with fall speeds of 1–2 m/s. An abrupt increase in fall speed occurs near the freezing level with fall speeds of 4–6 m/s typical of liquid droplets originating from the aggregates. The reflectivity increases abruptly there as well due to the increase in reflectivity of liquid water relative to ice.

The sounding shows warm, dry air in the range 1–4 km elevation with saturated air above this range and cooler, more moist air near the surface. This type of sounding was documented in stratiform rain regions by Zipser (1977) and is sometimes called an "onion sounding" due to its shape. The vertical mass flux profile shows descent in the lower troposphere and ascent at higher levels, as is characteristic of stratiform rain regions, though the transition level is somewhat higher than that usually documented. Ample lightning occurred in this system around the time of observation even though it was decaying.

Moisture convergence in this case is actually negative, as indicated in Table 1. Thus rainfall, which is an additional negative contributor to the moisture budget, is likely to be weak and transient, as expected in a stratiform situation.

3.2. 0909

Figure 3 portrays a rather different situation from 0825. The sounding has a dry, stable layer in the 3–7 km range, with a shallow but moist convective layer underlying it. The mass flux profile responds to this dry layer, with upward motion above 7 km and below 3.5 km, and net descent in between these two ascending layers. The dry

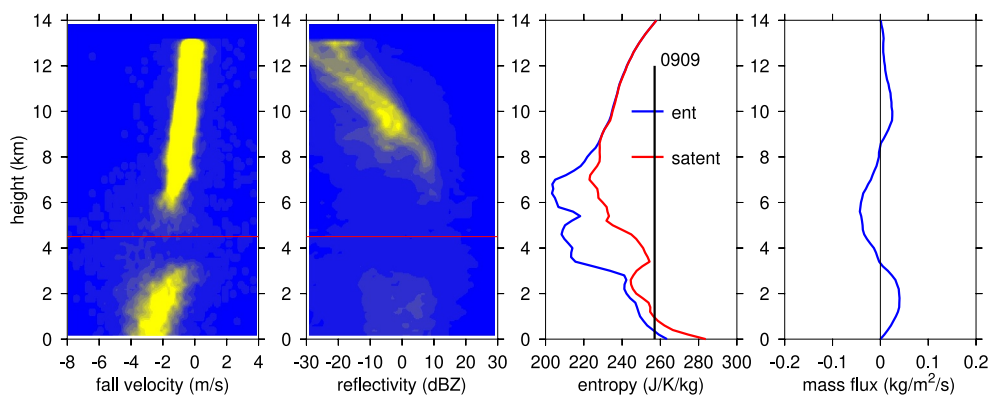

Figure 3. As in Figure 2 except Case 0909.

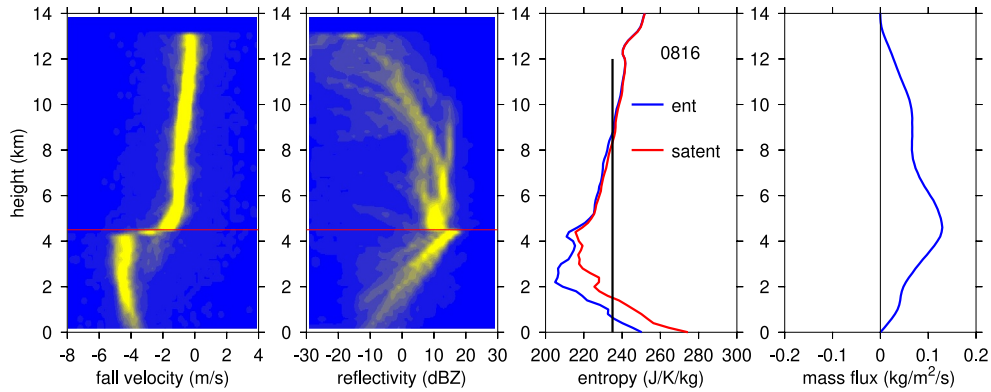

Figure 4. As in Figure 2 except Case 0816.

layer may be an elevated onion sounding associated with decaying deep convection and with shallow convective redevelopment below.

The satellite image for 0909 in Figure 1 indicates cloud top temperatures of 215–225 K and a loop of images supports the interpretation of a decaying system with redevelopment. The Doppler radar plot in Figure 3 shows little fallout of precipitation through the freezing level, suggesting strong evaporation in the dry air that extends up to 7 km in this case. However, a weak signal below 3 km is associated with shallow convective cells that appear in the radar time series (not shown). No lightning was observed in the vicinity of this system.

3.3. 0816

The particle fall velocity and reflectivity plots for 0816 (Figure 4) are similar to those of the classic stratiform case shown in Figure 2. However, as we shall see, this case couldn't be more different. The sounding for this case exhibits high column relative humidity and small but positive convective available potential energy (CAPE). The vertical mass flux is strongly upward at all levels but is bottom-heavy, with a maximum near 4 km. As Table 1 shows, the moisture convergence is 124 mm/day, which is much larger than the previous cases. A loop of the satellite images for this case shows the system to be nearly steady over a 4 hr period as it moves to the west, suggesting that the moisture tendency term is small, so that the precipitation rate is close to the moisture convergence. Cloud top temperatures are in the range 215–230 K, as in Case 0909.

The level of maximum parcel buoyancy in 0816 is near 4 km, with decreasing buoyancy above. This is consistent with the 4 km maximum in mass flux. The time series of particle fall speed is consistent with mostly aggregates above the freezing level with only a small region of graupel. A hint of this graupel can be seen in the fall velocity frequency distribution in Figure 4 between 2 and 4 km where a weak signal is seen with 2–3 m/s fall velocities. No lightning was observed in the vicinity of this system.

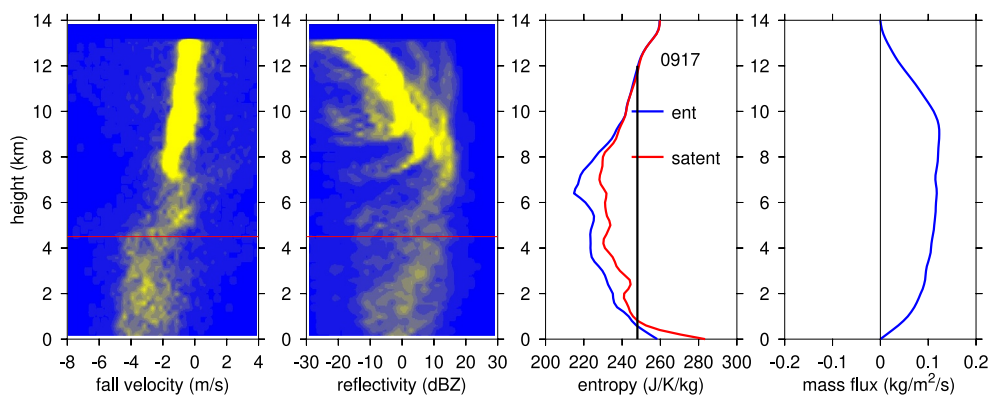

Figure 5. As in Figure 2 except Case 0917.

In summary, this is a case of deep convection with weak updrafts above the freezing level and most precipitation there in the form of aggregates. From the particle fall velocity and reflectivity distributions alone it would be hard to distinguish from the classical stratiform case, 0825. However, the mass flux profile, the moisture convergence, and the sounding are very different from 0825.

3.4. 0917

The 0917 case appears on infrared satellite imagery in Figure 1 to be similar to 0825, with minimum brightness temperatures near 200 K. However, a satellite loop shows this system to be in robust health rather than decaying. The sounding, shown for this system in Figure 5, exhibits high relative humidity, relatively large CAPE, and a level of maximum parcel buoyancy near 8 km. It thus differs significantly from 0816, as does the mass flux profile, which has a broad maximum over the 4–10 km range.

Unlike the other systems presented here, the particle fall velocity plot shows no jump in fall velocity at the freezing level, implying that the precipitation was primarily in the form of graupel. This system was observed to produce lightning. The moisture convergence in this system was a rather large 148 mm/day.

4. Discussion and Conclusions

We have shown that distinguishing aggregates from graupel above the freezing level is easily done with downward-pointing Doppler radars, as aggregates exhibit a sharp increase in fall velocity at the freezing level whereas graupel does not.

Aggregates above the freezing level are associated with a variety of situations in our results. Case 0825 represents a classic decaying stratiform system with weak upward motion above 7 km and weak downward motion below with a characteristic "onion" sounding. There is net moisture divergence. In contrast, Case 0816 exhibits a bottom-heavy mass flux profile, strong moisture convergence implying heavy rainfall, presumably due primarily to warm rain processes below the freezing level. Case 0909 is rather odd, with stratiform rain evaporating in a mid-level dry layer overlying a modest rainfall-producing layer at low levels. The mass flux profile in this case shows weak ascent at low and high levels with weak descent in the mid-level dry air. Case 0917 shows that graupel above the freezing level can occur in the study region and appears to be associated with maximum parcel buoyancy at high levels and deep vertical mass flux profiles.

Though aggregates are most easily detected by an abrupt increase in Doppler fall speed at the freezing level by W-band radars, they stand out in the longer wavelength but non-Doppler Ku band radars on TRMM (Kummerow et al., 1998) and Global Precipitation Measurement (GPM) (Hou et al., 2014) satellites as a bright band, that is, a narrow band of increased reflectivity at the freezing level. Houze et al. (2015) used the existence of bright bands as an indicator of stratiform rain regions, which they associated with the existence of aggregates above the freezing level. However, they suspected that this identification is potentially ambiguous, with alternative precipitation scenarios possibly occurring in some cases.

Our results support these suspicions and show that situations with widely varying precipitation rates and vertical mass flux profiles can occur with aggregates dominating above the freezing level. In particular, 0816 has deep but bottom-heavy convection and strong rainfall, with a radar signature nearly indistinguishable from that of the decaying stratiform Case 0825, which has only weak precipitation.

Inclusion in Global Research

We thank Marcial Garbanzo Salas and Ana María Durán Quesada of the University of Costa Rica for their help in facilitating OTREC flight operations out of Costa Rica. We also thank Germán Poveda and Manuel Zuluaga of the Universidad Nacional de Colombia in Medellín and Daniel Hernández Deckers of the Universidad Nacional in Bogotá for their hospitality and advice in understanding flight operations in and around Colombia.

Data Availability Statement

The 3DVar analyses used in this paper are available at Raymond (2021b). This analysis utilized Candis data analysis software, which is archived at Raymond (2021a). Two kilometer GOES-16 infrared satellite images for OTREC are archived at NCAR-OTREC-satellite (2019). HCR radar data may be obtained at NCAR-OTREC-

HCR (2019). GOES-16 Geostationary Lightning Mapper data are available at NOAA (2023). Figure generation is documented in Raymond (2024).

Acknowledgments
We thank the Earth Observing Laboratory of the National Center for Atmospheric Research for their excellent support of the OTREC project. We also thank Eric DeWeaver of the National Science Foundation for his wisdom in guiding us through a complex field program. Special thanks to Germán Poveda for sharing his knowledge about the Pacific coastal waters of Colombia and to Robert Houze for discussions about stratiform rain in this region. Finally, we thank the anonymous reviewer for many helpful comments. This work was supported by National Science Foundation, Directorate for Geosciences Grant 2414425.

References

Fuchs-Stone, Ž., Raymond, D. J., & Sentić, S. (2020). OTREC2019. Convection over the East Pacific and southwest Caribbean. *Geophysical Research Letters*, *47*(11), e2020GL087564. https://doi.org/10.1029/2020GL087564

Hou, A. Y., Kakar, R. K., Neeck, S., Azarbarzin, A. A., Kummerow, C. D., Kojima, M., et al. (2014). The global precipitation measurement mission. *Bulletin American Meteorological Society*, *95*(5), 701–722. https://doi.org/10.1175/BAMS-D-13-00164.1

Houze, R. A. (1977). Structure and dynamics of a tropical squall-line system. *Monthly Weather Review*, *105*(12), 1540–1567. https://doi.org/10.1175/1520-0493(1977)105<1540:sadoat>2.0.co;2

Houze, R. A., & Betts, A. K. (1981). Convection in GATE. *Reviews of Geophysics and Space Physics*, *19*(4), 541–574. https://doi.org/10.1029/rg019i004p00541

Houze, R. A., Rasmussen, K. L., Zuluaga, M. D., & Brodzik, S. R. (2015). The variable nature of convection in the tropics and subtropics: A legacy of 16 years of the tropical rainfall measuring mission satellite. *Reviews of Geophysics*, *53*(3), 994–1021. https://doi.org/10.1002/2015RG000488

Jaramillo, L., Poveda, G., & Mejía, J. (2017). Mesoscale convective systems and other precipitation features over the tropical Americas and surrounding seas as seen by TRMM. *International Journal of Climatology*, *37*(S1), 380–397. https://doi.org/10.1002/joc.5009

Kummerow, C., Barnes, W., Kozu, T., Shiue, J., & Simpson, J. (1998). The tropical rainfall measuring mission (TRMM) sensor package. *Journal of Atmospheric and Oceanic Technology*, *15*(3), 809–817. https://doi.org/10.1175/1520-0426(1998)015<0809:ttrmmt>2.0.co;2

Leary, C. A., & Houze, R. A. (1980). The contribution of mesoscale motions to the mass and heat fluxes of an intense tropical convective system. *Journal of the Atmospheric Sciences*, *37*(4), 784–796. https://doi.org/10.1175/1520-0469(1980)037<0784:tcommt>2.0.co;2

NCAR-OTREC-HCR. (2019). Hiaper cloud radar data for the OTREC project [Dataset]. *NCAR EOL*. Retrieved from https://catalog.eol.ucar.edu/otrec/radar

NCAR-OTREC-satellite. (2019). JPEG 2 km infrared satellite images for OTREC project. *NCAR EOL*. Retrieved from https://catalog.eol.ucar.edu/otrec/satellite

NOAA. (2023). NOAA GOES16 geostationary lightning mapper (GLM) data [Dataset]. *National Oceanic and Atmospheric Administration*. Retrieved from https://www.avl.class.noaa.gov/saa/products/search?datatype_family=GRGLMPROD

Poveda, G. (2023). Mechanisms controlling the 4D distribution of rainfall and latent heating over the rainiest region on Earth. *Journal of Geophysical Research*, *128*(23), e2023JD039328. https://doi.org/10.1029/2023JD039328

Poveda, G., & Mesa, O. J. (2000). On the existence of Lloró (the rainest locality on earth): Enhanced ocean-land-atmosphere interaction by a low-level jet. *Geophysical Research Letters*, *27*(11), 1675–1678. https://doi.org/10.1029/1999gl006091

Raymond, D. J. (2021a). Candis analysis and display software [Software]. *Zenodo*. https://doi.org/10.5281/zenodo.5150519

Raymond, D. J. (2021b). 3DVar analyses of dropsondes for OTREC project [Dataset]. *Zenodo*. https://doi.org/10.5281/zenodo.5152171

Raymond, D. J. (2024). *Documentation for figure generation in Raymond and Stone (2024)*. Zenodo. https://doi.org/10.5281/zenodo.14251905

Raymond, D. J., & Fuchs-Stone, Ž. (2021). Emergent properties of convection in OTREC and PREDICT. *Journal of Geophysical Research*, *126*(4), e2020JD033585. https://doi.org/10.1029/2020JD033585

Raymond, D. J., Stone, Ž., & Sentić, S. (2024). Rains and Showers in OTREC; Weak temperature gradient modeling. *Journal of Advances in Modeling Earth Systems*, *16*(3), e2023MS003980. https://doi.org/10.1029/2023MS003980

Sakamoto, M. S., Ambrizzi, T., & Poveda, G. (2011). Moisture sources and life cycle of convective systems over western Colombia. *Advances in Meteorology*, *2011*, 1–11. https://doi.org/10.1155/2011/890759

Zipser, E. J. (1969). The role of organized unsaturated convective downdrafts in the structure and rapid decay of an equatorial disturbance. *Journal of Applied Meteorology*, *8*(5), 799–814. https://doi.org/10.1175/1520-0450(1969)008<0799:troouc>2.0.co;2

Zipser, E. J. (1970). The Line Islands experiment, its place in tropical meteorology and the rise of the fourth school of thought. *Bulletin American Meteorological Society*, *51*(12), 1136–1146. https://doi.org/10.1175/1520-0477-51.12.1136

Zipser, E. J. (1977). Mesoscale and convective scale downdrafts as distinct components of squall-line structure. *Monthly Weather Review*, *105*(12), 1568–1589. https://doi.org/10.1175/1520-0493(1977)105<1568:macdad>2.0.co;2